Eur. Phys. J. Plus (2017) **132**: 499
DOI 10.1140/epjp/i2017-11794-y

THE EUROPEAN PHYSICAL JOURNAL PLUS

Regular Article

Graphene coherent states

Erik Díaz-Bautista[a] and David J. Fernández[b]

Physics Department, Cinvestav, P.O. Box. 14-740, 07000 Mexico City, Mexico

Received: 2 September 2017 / Revised: 21 October 2017
Published online: 29 November 2017 –

Abstract. In this paper we will construct the coherent states for a Dirac electron in graphene placed in a constant homogeneous magnetic field which is orthogonal to the graphene surface. First of all, we will identify the appropriate annihilation and creation operators. Then, we will derive the coherent states as eigenstates of the annihilation operator, with complex eigenvalues. Several physical quantities, as the Heisenberg uncertainty product, probability density and mean energy value, will be as well explored.

1 Introduction

In the quantum mechanical treatment of the harmonic oscillator, the first task typically is to determine the eigenstates and eigenvalues of the Hamiltonian, looking for them either by solving the corresponding second-order ordinary differential equation with appropriate boundary conditions or through algebraic techniques. It is just when analyzing the result of the calculation for the mean values of the position and momentum operators in these states, both becoming zero, that one realizes the impossibility of choosing directly the bound states as semiclassical models (see *e.g.*, [1]). This is why Schrödinger looked for an alternative set of states, whose mean values would follow the oscillator classical trajectory in phase space [2]; nowadays they are called coherent states (CS), after Glauber coined the name in the sixties of the previous century, based on the coherence properties of these states [3,4]. The CS have proved very fruitful in several areas of physics, *e.g.*, the coherent states are used often to analyze the border between classical and quantum mechanics (the so-called semiclassical regime), they have been employed as models of light in quantum optics, they supply alternatives to the coordinates or momentum representations, they have shed light onto the quantization procedures, etc. [5–8]. Retrospectively, one can observe that the coherent state approach represents an important second stage in the study of a quantum mechanical system.

There are several coherent state definitions for systems different from the harmonic oscillator (see, *e.g.*, [7]); thus, to proceed with a CS analysis first one has to fix the definition to be used: whenever is possible to identify an annihilation operator of the system, the coherent states which are eigenstates of such an operator seems the most natural available choice.

On the other hand, it is well known that graphene is a single layer of carbon atoms arranged in a hexagonal honeycomb lattice, which is the basic structural element of other carbon allotropes. Since its conduction and valence bands meet at the so-called Dirac points on the edge of the Brillouin zone (see fig. 1), it is considered a zero-gap semiconductor [9–14].

At low energies, close to a Dirac point, the electrons can be described by an equation which is formally equivalent to the massless (or ultra-relativistic) Dirac equation:

$$-i\hbar\, v_F\, \boldsymbol{\sigma} \cdot \nabla \Psi(\mathbf{r}) = E\Psi(\mathbf{r}), \tag{1}$$

where $v_F \sim 10^6$ m/s is the Fermi velocity, which replaces the velocity of light in Dirac theory, the components of the vector $\boldsymbol{\sigma}$ are the Pauli matrices, $\Psi(\mathbf{r})$ is the two-component wave function of the electrons and E is its energy [15].

Consequently, the electrons and holes in graphene are called Dirac fermions [16–22], which emerge naturally from a tight-binding model for a generic hexagonal lattice in the low-energy regime [23]. In fact, graphene belongs to a class of systems in condensed matter for which the low-energy quasi-particles behave like massless or massive Dirac fermions. These systems are known as Dirac materials in the literature [24].

It is worth to notice that, when Dirac fermions are compared with ordinary electrons in magnetic fields, their behavior leads to new physical phenomena, such as the anomalous integer quantum Hall effect, the Zitterbewegung

[a] e-mail: ediaz@fis.cinvestav.mx
[b] e-mail: david@fis.cinvestav.mx

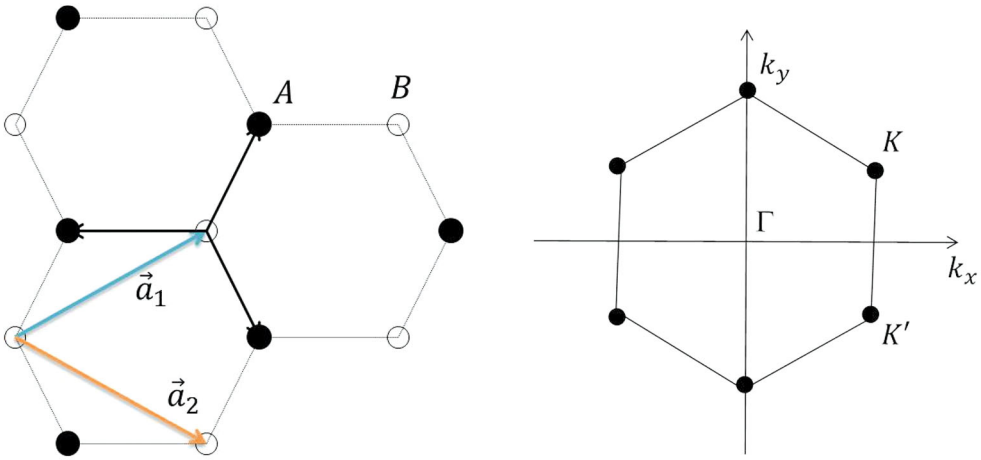

Fig. 1. Left: Lattice structure of the graphene, where the sublattices are labeled by A and B. Right: Brillouin zone for the graphene. The Dirac cones appear at the K and K' points.

and the Klein paradox [16,25]. We shall see below that under particular physical conditions, a problem similar to that considered in [26] will arise naturally. Motivated by this, it seems clear to us the need to build up the coherent states for graphene in static magnetic fields, *i.e.*, to address already the second stage in the quantum mechanical analysis of this problem. Let us note that, up to now, the only work we have detected in which the CS for this system have been studied, for a strong homogeneous magnetic field, was done by Wu *et al.* through group theoretical methods [27].

In order to start implementing our program, this paper has been organized as follows. In sect. 2 the Dirac-Weyl equation will be introduced and the physical problem to be considered will be briefly discussed. In sect. 3 the annihilation operator associated to our system will be defined, and the corresponding coherent states will be constructed as eigenstates of that operator. We will analyze as well several physical quantities for these states. Our conclusions will be presented in sect. 4.

2 Dirac-Weyl equation

Let us suppose that the graphene is placed in a static magnetic field which is orthogonal to the material surface (the $x-y$ plane) [15,28,29]. The interaction of a Dirac electron with such a field close to a Dirac point K in the Brillouin zone is described by the Dirac-Weyl equation, which is obtained by replacing in eq. (1) the momentum operator $\boldsymbol{p} = -i\hbar\nabla$ by $\boldsymbol{p} + e\boldsymbol{A}/c$, leading to

$$v_F\,\boldsymbol{\sigma}\cdot\left(\boldsymbol{p}+\frac{e\boldsymbol{A}}{c}\right)\Psi(x,y) = E\Psi(x,y), \tag{2}$$

where $-e$ is the charge of the electron. Landau gauge is conveniently chosen, with the vector potential given by $\boldsymbol{A} = A(x)\hat{e}_y$ and $\boldsymbol{B} = \nabla\times\boldsymbol{A} = B(x)\hat{e}_z$. Note that there is a translational invariance along the y-direction, then the spinor $\Psi(x,y)$ can be expressed as

$$\Psi(x,y) = \exp(iky)\begin{pmatrix}\psi^+(x)\\ i\psi^-(x)\end{pmatrix}, \tag{3}$$

with k being the wave number in the y-direction and $\psi^{\pm}(x)$ describing the electron amplitude on two adjacent sites in the unit cell of graphene. Thus, the solutions of the Dirac-Weyl equation have an internal degree of freedom that mimics the spin, called pseudospin. It admits the interpretation that each component is the projection of the particle wavefunction onto the sublattice A (spin up) or B (spin down).

Substituting now eq. (3) in eq. (2), the Dirac-Weyl equation yields two coupled first-order linear differential equations,

$$\left(\pm\frac{\mathrm{d}}{\mathrm{d}x}+\frac{e}{c\hbar}A(x)+k\right)\psi^{\mp}(x) = \frac{E}{\hbar\,v_F}\psi^{\pm}(x), \tag{4}$$

which can be easily decoupled into two Schrödinger equations $H^{\pm}\psi^{\pm}(x) = \mathcal{E}\psi^{\pm}(x)$, where [29]

$$H^{\pm} = -\frac{\mathrm{d}^2}{\mathrm{d}x^2}+V^{\pm},\qquad V^{\pm} = \left(\frac{eA(x)}{c\hbar}+k\right)^2 \pm \frac{e}{c\hbar}\frac{\mathrm{d}A(x)}{\mathrm{d}x},\qquad \mathcal{E} = \frac{E^2}{\hbar^2 v_F^2}. \tag{5}$$

For a constant magnetic field, orthogonal to the graphene surface and pointing in the positive z-direction ($\boldsymbol{B} = B_0\hat{e}_z$ with $B_0 > 0$), the vector potential is selected as $\boldsymbol{A} = B_0 x\hat{e}_y$. Introducing now the constant ω as

$$B_0 = \frac{c\hbar}{2e}\omega \quad \rightarrow \quad \omega = \frac{2eB_0}{c\hbar},$$

whose dimensions are (lenght)$^{-2}$, the potentials in eq. (5) become two shifted oscillators of the form

$$V^{\pm} = \frac{\omega^2}{4}\left(x + \frac{2k}{\omega}\right)^2 \pm \frac{1}{2}\omega. \tag{6}$$

Thus, the eigenvalues $\mathcal{E}_n^{\pm}$ for the Hamiltonians $H^{\pm}$ are related as follows:

$$\mathcal{E}_0^- = 0, \quad \mathcal{E}_n^- = \mathcal{E}_{n-1}^+ = n\omega, \quad n = 1, 2, \ldots, \tag{7}$$

and the associated eigenfunctions are those of the standard harmonic oscillator,

$$\psi_n^{\pm}(x) = \sqrt{\frac{1}{2^n n!}\left(\frac{\omega}{2\pi}\right)^{1/2}} H_n\left[\sqrt{\frac{\omega}{2}}\left(x + \frac{2k}{\omega}\right)\right] \exp\left(-\frac{\omega}{4}\left(x + \frac{2k}{\omega}\right)^2\right), \tag{8}$$

where $H_n[\cdot]$ denotes the Hermite polynomial of degree $n \in \mathbb{N}$.

We conclude that the complete solution of the corresponding Dirac-Weyl equation in a constant magnetic field consists of the eigenvalues

$$E_n^{\pm} = \pm\hbar\, v_F\sqrt{n\omega}, \quad n = 0, 1, \ldots, \tag{9}$$

where the plus (minus) sign refers to the enegy electrons (holes), and the normalized eigenvectors

$$\Psi_0(x, y) = \exp(iky)\begin{pmatrix} 0 \\ i\,\psi_0^-(x) \end{pmatrix}, \quad \Psi_n(x, y) = \frac{\exp(iky)}{\sqrt{2}}\begin{pmatrix} \psi_{n-1}^+(x) \\ i\,\psi_n^-(x) \end{pmatrix}, \quad n = 1, 2, \ldots . \tag{10}$$

3 Annihilation operator

Since the eigenstates of the previous Dirac-Weyl equation are expressed in terms of the eigenfunctions of the standard harmonic oscillator, it seems natural to look for an annihilation operator for the Hamiltonian in eq. (2). In fact, let $\hat{A}^-$ be the operator defined by

$$\hat{A}^- = \begin{pmatrix} f_1(\hat{N})\hat{\vartheta}^- & 0 \\ 0 & f(\hat{N} + \hat{1})\hat{\vartheta}^- \end{pmatrix}, \tag{11}$$

where $\hat{\vartheta}^{\pm}$, $\hat{N}$ are given by

$$\hat{\vartheta}^- = \frac{1}{\sqrt{2}}\left(z + \partial_z\right), \qquad \hat{\vartheta}^+ = \frac{1}{\sqrt{2}}\left(z - \partial_z\right), \qquad \hat{N} = \hat{\vartheta}^+\hat{\vartheta}^-,$$

with $z = \sqrt{\omega/2}\,(x + 2k/\omega)$, and f, f_1 are two real adjustable functions which will be used to guarantee that $\hat{A}^-\Psi_n = c_n\Psi_{n-1}$. Then,

$$\hat{A}^-\Psi_n = \begin{cases} 0 & \text{for } n = 0 \\ \dfrac{f(1)}{\sqrt{2}}\Psi_0 & \text{for } n = 1 \\ \dfrac{1}{\sqrt{2}}\exp(iky)\begin{pmatrix} \sqrt{n-1}f_1(n-2)\psi_{n-2} \\ \sqrt{n}f(n)i\psi_{n-1} \end{pmatrix} & \text{for } n = 2, 3, \ldots . \end{cases} \tag{12}$$

In order to ensure that

$$\hat{A}^-\Psi_n = c_n\Psi_{n-1}, \tag{13}$$

it must happen that

$$\sqrt{n-1}f_1(n-2) = \sqrt{n}f(n), \quad n = 2, 3, \ldots . \tag{14}$$

In such a case it is obtained that

$$c_n = \begin{cases} 0 & \text{for } n = 0, \\ \dfrac{f(1)}{\sqrt{2}} & \text{for } n = 1, \\ \sqrt{n} f(n) & \text{for } n = 2, 3, \ldots, \end{cases} \tag{15}$$

and the explicit expression for the annihilation operator $\hat{A}^-$ turns out to be

$$\hat{A}^- = \begin{pmatrix} \dfrac{\sqrt{\hat{N}+\hat{2}}}{\sqrt{\hat{N}+\hat{1}}} f(\hat{N}+\hat{2})\hat{\vartheta}^- & 0 \\ 0 & f(\hat{N}+\hat{1})\hat{\vartheta}^- \end{pmatrix}. \tag{16}$$

Equation (15) indicates that the explicit form of the function $f(n)$ is required to determine the complete action of the annihilation operator $\hat{A}^-$ onto the eigenstates Ψ_n. It is also quite important for the properties of the graphene coherent states, as it will be immediately seen.

3.1 Coherent states as eigenvectors of $\hat{\mathbf{A}}^-$

Let us define the coherent states Ψ_α as eigenstates of the annihilation operator $\hat{A}^-$ with complex eigenvalue α

$$\hat{A}^- \Psi_\alpha = \alpha \Psi_\alpha, \quad \alpha \in \mathbb{C}. \tag{17}$$

Expressing Ψ_α as a linear combination of the states Ψ_n, we have

$$\Psi_\alpha(x,y) = \sum_{n=0}^{\infty} a_n \Psi_n(x,y) = \left[a_0 \begin{pmatrix} 0 \\ i\psi_0^-(x) \end{pmatrix} + \sum_{n=1}^{\infty} \frac{a_n}{\sqrt{2}} \begin{pmatrix} \psi_{n-1}^+(x) \\ i\psi_n^-(x) \end{pmatrix} \right] \exp(iky). \tag{18}$$

Using eq. (17) we find a recurrence relation for the coefficients a_n which depends on the value taken by $f(1)$. We can identify two different cases.

3.1.1 Case with $f(1) \neq 0$

First of all suppose that $f(n) \neq 0 \ \forall \ n = 1, 2, \ldots$. Thus we get $a_1 = \sqrt{2}\alpha a_0 / f(1)$ and

$$a_{n+1} = \frac{\alpha^n \, a_1}{\sqrt{(n+1)!} f(n+1) \cdots f(2)} = \frac{\sqrt{2}\, \alpha^{n+1} \, a_0}{\sqrt{(n+1)!}\, [f(n+1)]!}, \tag{19}$$

where

$$[f(n)]! \equiv \begin{cases} 1 & \text{for } n = 0, \\ f(1) \cdots f(n) & \text{for } n = 1, 2, \ldots . \end{cases}$$

The free constant a_0 is used to normalize Ψ_α; we obtain:

$$\Psi_\alpha(x,y) = \left[1 + \sum_{n=1}^{\infty} \frac{2\,|\alpha|^{2n}}{n!\,([f(n)]!)^2} \right]^{-1/2} \left[\Psi_0(x,y) + \sum_{n=1}^{\infty} \frac{\sqrt{2}\,\alpha^n}{\sqrt{n!}\,[f(n)]!} \Psi_n(x,y) \right]. \tag{20}$$

3.1.2 Case with $f(1) = 0$

If $f(1) = 0$ we obtain that $a_0 = 0$ and the following recurrence relationship:

$$a_{n+1} \sqrt{n+1}\, f(n+1) = \alpha \, a_n, \quad n = 1, 2, \ldots . \tag{21}$$

Now, depending on the value of $f(2)$, two possibilities appear once again.

A. Case with $f(2) \neq 0$.
If we suppose that $f(n) \neq 0\ \forall\ n = 2, 3, \ldots$ and define $g(n) \equiv f(n+1)$, eq. (21) leads to

$$a_{n+1} = \frac{\alpha^n}{\sqrt{(n+1)!}[g(n)]!} a_1. \tag{22}$$

Substituting this expression in eq. (18) and then normalizing we obtain

$$\Psi_\alpha(x,y) = \left[\sum_{n=0}^{\infty} \frac{|\alpha|^{2n}}{(n+1)!\,([g(n)]!)^2}\right]^{-1/2} \sum_{n=0}^{\infty} \frac{\alpha^n}{\sqrt{(n+1)!}\,[g(n)]!} \Psi_{n+1}(x,y). \tag{23}$$

B. Case with $f(2) = 0$.
On the other hand, if $f(2) = 0$ and $f(n) \neq 0\ \forall\ n = 3, 4, \ldots$, the normalized coherent states turn out to be now

$$\Psi_\alpha(x,y) = \left[\sum_{n=0}^{\infty} \frac{|\alpha|^{2n}}{(n+2)!\,([h(n)]!)^2}\right]^{-1/2} \sum_{n=0}^{\infty} \frac{\alpha^n}{\sqrt{(n+2)!}\,[h(n)]!} \Psi_{n+2}(x,y), \tag{24}$$

where $h(n) \equiv f(n+2)$.

Let us notice that the graphene coherent states of eqs. (20), (23), (24) look similar to the so-called vector coherent states. For information concerning the last states, the reader can refer to, *e.g.*, [30–32] and references therein.

3.2 Mean values and the Heisenberg uncertainty relation

Let the dimensionless position and momentum operators be given by

$$\hat{z} = \frac{1}{\sqrt{2}}(\hat{\vartheta}^+ + \hat{\vartheta}^-), \qquad \hat{p} = \frac{i}{\sqrt{2}}(\hat{\vartheta}^+ - \hat{\vartheta}^-). \tag{25}$$

In units of $\hbar$, the Heisenberg uncertainty relation is expressed by

$$\sigma_z^2 \sigma_p^2 \geq \frac{1}{4}, \tag{26}$$

where $\sigma_S^2 \equiv \langle \hat{S}^2 \rangle - \langle \hat{S} \rangle^2$ for an arbitrary observable $\hat{S}$.

We will calculate next these quantities for some examples of the coherent states, which will stress the important role played by the function $f(n)$ in our treatment.

3.2.1 The case with $f(1) \neq 0$

Let us consider first the particular choice $f(\hat{N}) = \hat{1}$. Thus, eq. (20) leads to

$$\Psi_\alpha(x,y) = \frac{1}{\sqrt{2\exp(r^2) - 1}} \left[\Psi_0(x,y) + \sum_{n=1}^{\infty} \frac{\sqrt{2}\alpha^n}{\sqrt{n!}} \Psi_n(x,y)\right], \tag{27}$$

where $r = |\alpha|$.

Using these coherent states, the mean values for the operators $\hat{z}$, $\hat{p}$ of eq. (25) as well as their squares become

$$\langle \hat{z} \rangle_\alpha = \frac{\sqrt{2}\mathbf{Re}(\alpha)}{2\exp(r^2) - 1} \left[\exp(r^2) + \sum_{n=1}^{\infty} \frac{r^{2n}}{\Gamma(n)\Gamma(n+2)}\right], \tag{28a}$$

$$\langle \hat{z}^2 \rangle_\alpha = \frac{1}{4\exp(r^2) - 2} \left[1 + 4r^2\exp(r^2) + 2[[\mathbf{Re}(\alpha)]^2 - [\mathbf{Im}(\alpha)]^2] \left(\exp(r^2) + \sum_{n=1}^{\infty} \frac{\sqrt{n+1}r^{2n}}{\Gamma(n)\Gamma(n+3)}\right)\right], \tag{28b}$$

$$\langle \hat{p} \rangle_\alpha = \frac{\sqrt{2}\mathbf{Im}(\alpha)}{2\exp(r^2) - 1} \left[\exp(r^2) + \sum_{n=1}^{\infty} \frac{r^{2n}}{\Gamma(n)\Gamma(n+2)}\right], \tag{28c}$$

$$\langle \hat{p}^2 \rangle_\alpha = \frac{1}{4\exp(r^2) - 2} \left[1 + 4r^2\exp(r^2) - 2[[\mathbf{Re}(\alpha)]^2 - [\mathbf{Im}(\alpha)]^2] \left(\exp(r^2) + \sum_{n=1}^{\infty} \frac{\sqrt{n+1}r^{2n}}{\Gamma(n)\Gamma(n+3)}\right)\right]. \tag{28d}$$

Through them it is straightforward to calculate $(\sigma_z)_\alpha^2 (\sigma_p)_\alpha^2$ (see fig. 2). Note that in the limit $\alpha \to 0$ we have $(\sigma_z)_\alpha^2 (\sigma_p)_\alpha^2 \to 1/4$.

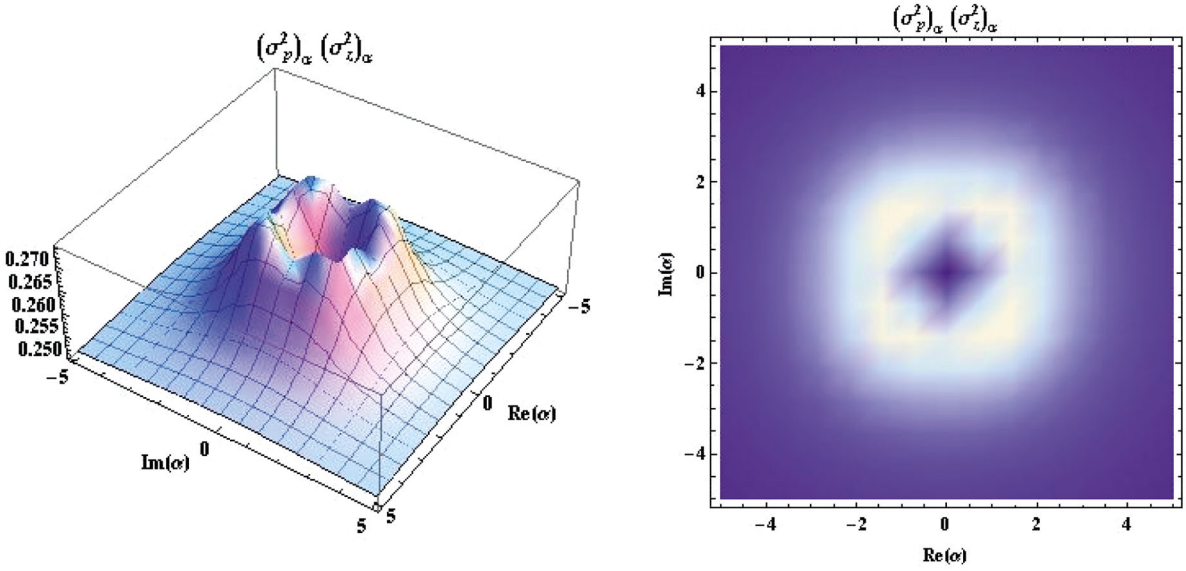

Fig. 2. Heisenberg uncertainty relation $(\sigma_z)^2_\alpha(\sigma_p)^2_\alpha$ as function of α for $f(n) = 1$.

3.2.2 The case with $f(1) = 0$

As we saw in sect. 3.1.2, when $f(1) = 0$ two options appear, which depend on the value taken by $f(2)$.

A. The case with $f(2) \neq 0$.

Let us choose now $f(\hat{N}+\hat{1}) = g(\hat{N}) = \frac{\sqrt{\hat{N}}}{\sqrt{\hat{N}+\hat{1}}}$, so that $f(n) \neq 0\ \forall\ n = 2, 3, \ldots$. From eq. (23), the explicit form for the normalized coherent states becomes

$$\Psi_\alpha(x,y) = \exp(-r^2/2)\sum_{n=0}^{\infty}\frac{\alpha^n}{\sqrt{n!}}\Psi_{n+1}(x,y). \tag{29}$$

The mean values for the operators of eq. (25) and their squares become

$$\langle\hat{z}\rangle_\alpha = \frac{\mathbf{Re}(\alpha)}{\sqrt{2}}\left[1+\exp(-r^2)\sum_{n=0}^{\infty}\frac{\sqrt{n+2}\,r^{2n}}{\sqrt{\Gamma(n+1)\Gamma(n+2)}}\right], \tag{30a}$$

$$\langle\hat{z}^2\rangle_\alpha = \exp(-r^2)\sum_{n=0}^{\infty}\frac{(n+1)r^{2n}}{\Gamma(n+1)} + \frac{[[\mathbf{Re}(\alpha)]^2-[\mathbf{Im}(\alpha)]^2]}{2}\left(1+\exp(-r^2)\sum_{n=0}^{\infty}\frac{\sqrt{n+3}\,r^{2n}}{\sqrt{\Gamma(n+1)\Gamma(n+2)}}\right), \tag{30b}$$

$$\langle\hat{p}\rangle_\alpha = \frac{\mathbf{Im}(\alpha)}{\sqrt{2}}\left[1+\exp(-r^2)\sum_{n=0}^{\infty}\frac{\sqrt{n+2}\,r^{2n}}{\sqrt{\Gamma(n+1)\Gamma(n+2)}}\right], \tag{30c}$$

$$\langle\hat{p}^2\rangle_\alpha = \exp(-r^2)\sum_{n=0}^{\infty}\frac{(n+1)r^{2n}}{\Gamma(n+1)} - \frac{[[\mathbf{Re}(\alpha)]^2-[\mathbf{Im}(\alpha)]^2]}{2}\left(1+\exp(-r^2)\sum_{n=0}^{\infty}\frac{\sqrt{n+3}\,r^{2n}}{\sqrt{\Gamma(n+1)\Gamma(n+2)}}\right). \tag{30d}$$

In the limit $\alpha \to 0$ it turns out that $(\sigma_z)^2_\alpha(\sigma_p)^2_\alpha \to 1$ (see fig. 3).

B. The case with $f(2) = 0$.

Let us consider finally that $f(\hat{N}+\hat{2}) = h(\hat{N}) = \frac{\hat{N}\sqrt{\hat{N}+\hat{1}}}{\sqrt{\hat{N}+\hat{2}}}$. The explicit expression for the normalized coherent states arises from eq. (24):

$$\Psi_\alpha(x,y) = \frac{1}{\sqrt{{}_0F_2(1,2;r^2)}}\sum_{n=0}^{\infty}\frac{\alpha^n}{n!\sqrt{(n+1)!}}\Psi_{n+2}(x,y), \tag{31}$$

where ${}_pF_q$ is a generalized hypergeometric function defined by

$${}_pF_q(a_1,\ldots,a_p,b_1,\ldots,b_q;x) = \frac{\Gamma(b_1)\ldots\Gamma(b_q)}{\Gamma(a_1)\ldots\Gamma(a_p)}\sum_{n=0}^{\infty}\frac{\Gamma(a_1+n)\ldots\Gamma(a_p+n)}{\Gamma(b_1+n)\ldots\Gamma(b_q+n)}\frac{x^n}{n!}\,.$$

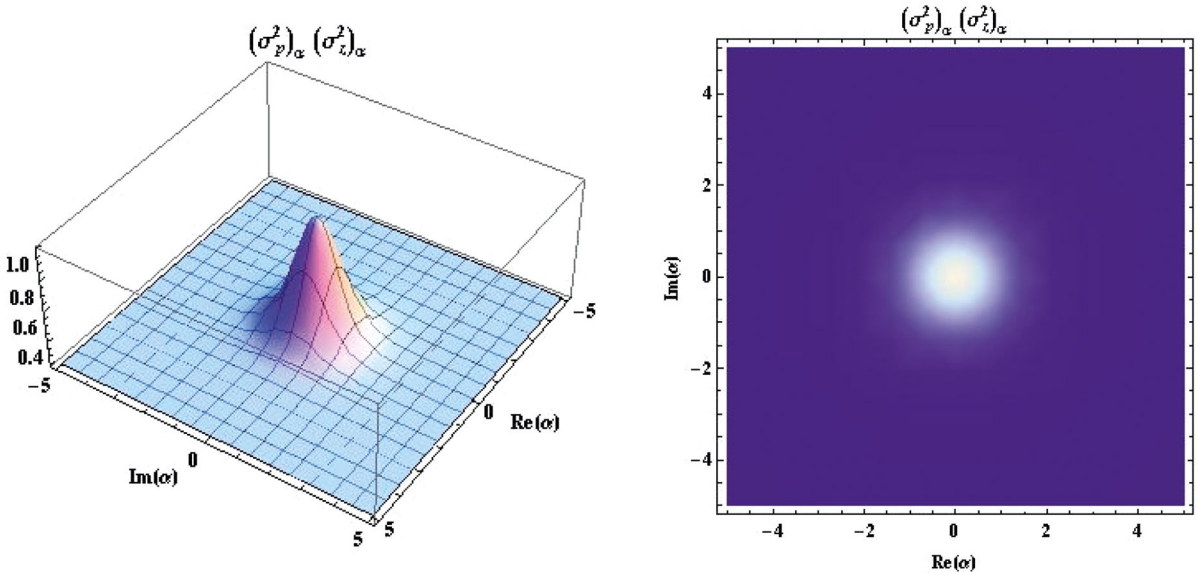

Fig. 3. Heisenberg uncertainty relation $(\sigma_z)^2_\alpha(\sigma_p)^2_\alpha$ as function of α for $f(n) = \sqrt{n-1}/\sqrt{n}$.

The mean values for the operators in eq. (25) and their squares are now

$$\langle\hat{z}\rangle_\alpha = \frac{\mathbf{Re}(\alpha)}{\sqrt{2}\,{}_0F_2(1,2;r^2)}\left[{}_0F_2(2,2;r^2) + \sum_{n=0}^{\infty}\frac{\sqrt{n+3}\,r^{2n}}{n!\sqrt{[\Gamma(n+2)]^3\Gamma(n+3)}}\right], \tag{32a}$$

$$\langle\hat{z}^2\rangle_\alpha = \frac{1}{2\,{}_0F_2(1,2;r^2)}\left[2\sum_{n=0}^{\infty}\frac{(n+2)r^{2n}}{\Gamma(n+2)[\Gamma(n+1)]^2} + [[\mathbf{Re}(\alpha)]^2 - [\mathbf{Im}(\alpha)]^2] \times\left(\frac{{}_0F_2(2,3;r^2)}{2} + \sum_{n=0}^{\infty}\frac{\sqrt{n+3}\,r^{2n}}{\Gamma(n+1)\sqrt{\Gamma(n+2)[\Gamma(n+3)]^3}}\right)\right], \tag{32b}$$

$$\langle\hat{p}\rangle_\alpha = \frac{\mathbf{Im}(\alpha)}{\sqrt{2}\,{}_0F_2(1,2;r^2)}\left[{}_0F_2(2,2;r^2) + \sum_{n=0}^{\infty}\frac{\sqrt{n+3}\,r^{2n}}{n!\sqrt{[\Gamma(n+2)]^3\Gamma(n+3)}}\right], \tag{32c}$$

$$\langle\hat{p}^2\rangle_\alpha = \frac{1}{2\,{}_0F_2(1,2;r^2)}\left[2\sum_{n=0}^{\infty}\frac{(n+2)r^{2n}}{\Gamma(n+2)[\Gamma(n+1)]^2} - [[\mathbf{Re}(\alpha)]^2 - [\mathbf{Im}(\alpha)]^2] \times\left(\frac{{}_0F_2(2,3;r^2)}{2} + \sum_{n=0}^{\infty}\frac{\sqrt{n+3}\,r^{2n}}{\Gamma(n+1)\sqrt{\Gamma(n+2)[\Gamma(n+3)]^3}}\right)\right]. \tag{32d}$$

In the limit $\alpha \to 0$ we get $(\sigma_z)^2_\alpha(\sigma_p)^2_\alpha \to 4$ (see fig. 4).

As we can see, the Heisenberg uncertainty relation depends strongly on the coherent states under consideration. Thus, for the states in eq. (27) it takes its minimum at $\alpha = 0$, while for those in eqs. (29) and (31) their maxima are reached at the same point; this is so since the lowest-energy eigenstate involved in the corresponding linear combination is different if different families of coherent states are taken into account (see also [33–35]).

3.3 Magnetic field and probability density

The probability density $\rho = \Psi_\alpha^\dagger\Psi_\alpha$ will be used to analyze the properties of the graphene coherent states. It will depend on the following matrix elements [28]:

$$\rho_{n,m}(x) := \psi^+_{n-1}(x)\psi^+_{m-1}(x) + \psi^-_n(x)\psi^-_m(x) = \rho_{m,n}(x). \tag{33}$$

Note also that, according to eq. (8), it depends on the magnetic field intensity B_0 through the parameter ω.

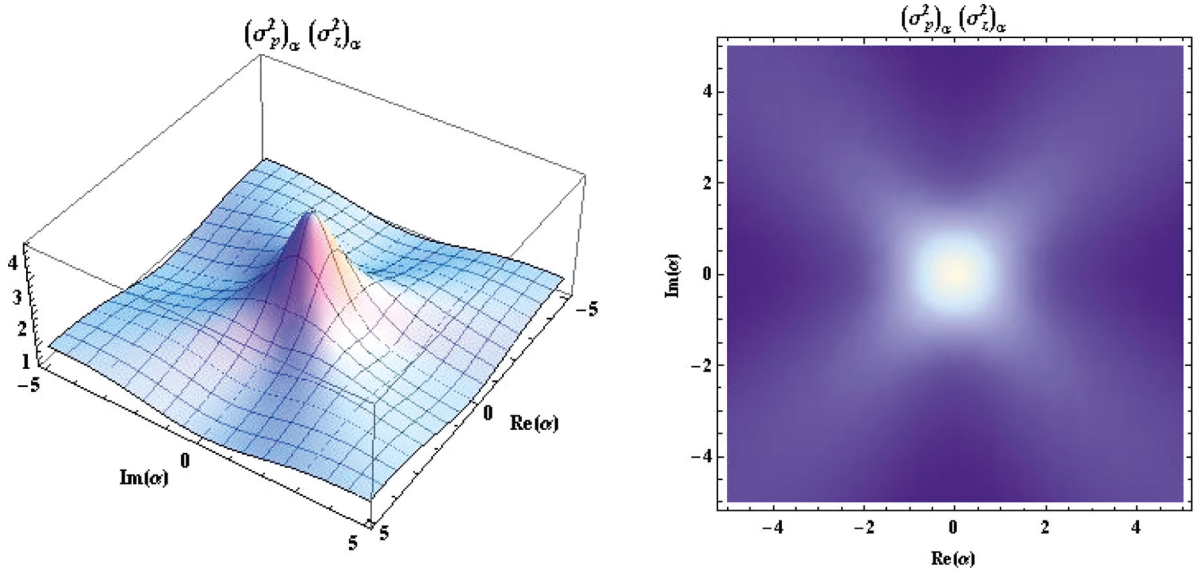

Fig. 4. Heisenberg uncertainty relation $(\sigma_z)^2_\alpha(\sigma_p)^2_\alpha$ as function of α for $f(n) = (n-2)\sqrt{n-1}/\sqrt{n}$.

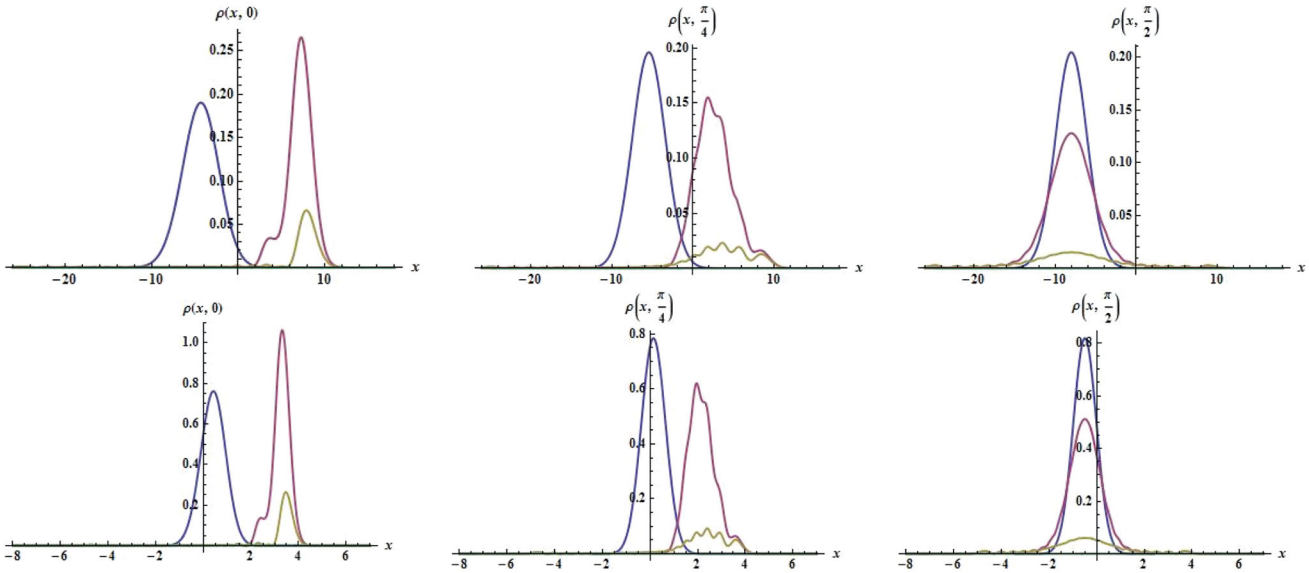

Fig. 5. Probability density $\rho(x, r, \theta)$ for $f(n) = 1$ with $B_0 = 1/8$ (above), $B_0 = 2$ (below), $\theta = 0$, $\pi/4$, $\pi/2$ (left to right, respectively) and $k = 1$. The blue, red and brown lines correspond to $r = 1, 4, 5$, respectively.

3.3.1 Probability density for $f(1) \neq 0$

A straightforward calculation using eq. (27) leads to

$$\rho(x,r,\theta) = \frac{1}{2\exp(r^2)-1}\left[\sum_{m=1}^{\infty}\sum_{n=1}^{\infty}\frac{r^{m+n}\cos{(n-m)\theta}}{\sqrt{m!\,n!}}\rho_{n,m}(x) + 2\sum_{n=1}^{\infty}\frac{r^n\cos(n\theta)}{\sqrt{n!}}\psi_n^-(x)\psi_0^-(x) + (\psi_0^-(x))^2\right], \quad (34)$$

where $\theta = \mathrm{Arg}[\alpha]$, $r = |\alpha|$. Plots of this probability density for two magnetic field intensities and different θ's and r's are shown in fig. 5.

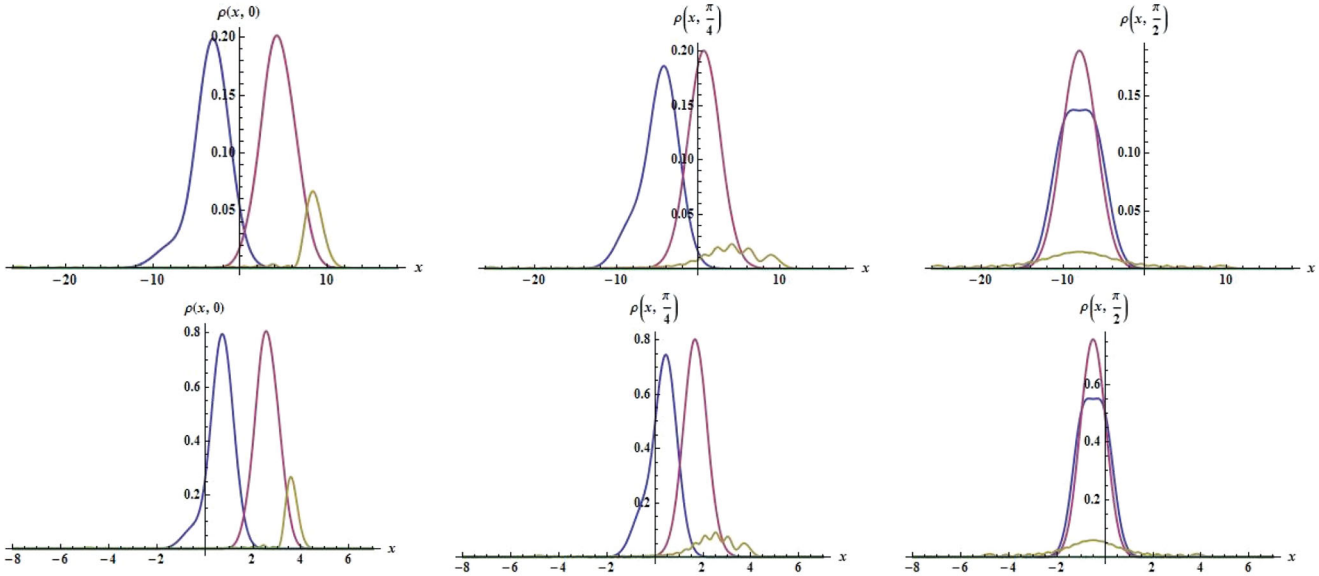

Fig. 6. Probability density $\rho(x, r, \theta)$ for $f(n) = \sqrt{n-1}/\sqrt{n}$ with $B_0 = 1/8$ (above), $B_0 = 2$ (below), $\theta = 0$, $\pi/4$, $\pi/2$ (left to right, respectively) and $k = 1$. The blue, red and brown lines correspond to $r = 1, 3, 5$, respectively.

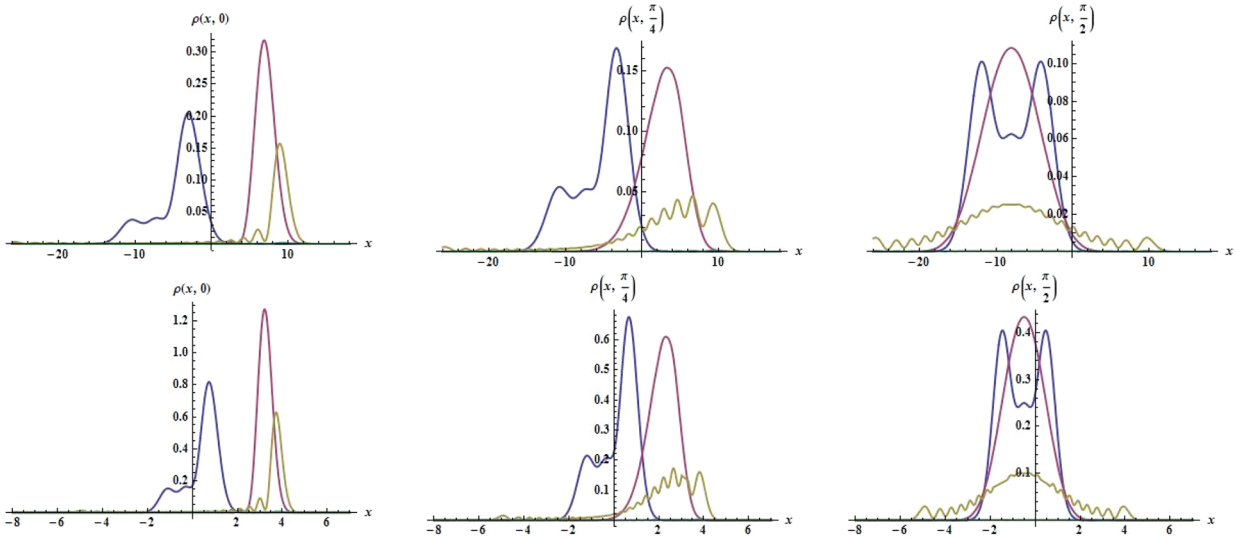

Fig. 7. Probability density $\rho(x, r, \theta)$ for $f(n) = (n-2)\sqrt{n-1}/\sqrt{n}$ with $B_0 = 1/8$ (above), $B_0 = 2$ (below), $\theta = 0$, $\pi/4$, $\pi/2$ (left to right, respectively), and $k = 1$. The blue, red and brown lines correspond to $r = 1, 50, 100$, respectively.

3.3.2 Probability density for $f(1) = 0$

A. Case with $f(2) \neq 0$.
On the other hand, for the states of eq. (29) we get (see fig. 6)

$$\rho(x, r, \theta) = \frac{\exp(-r^2)}{2} \sum_{m=0}^{\infty} \sum_{n=0}^{\infty} \frac{r^{m+n} \cos{(n-m)\theta}}{\sqrt{\Gamma(m+1)\Gamma(n+1)}} \rho_{n+1,m+1}(x). \tag{35}$$

B. Case with $f(2) = 0$.
Finally, by employing the states of eq. (31) we arrive at (see fig. 7)

$$\rho(x, r, \theta) = \frac{1}{2\,{}_0F_2(1, 2; r^2)} \sum_{m=0}^{\infty} \sum_{n=0}^{\infty} \frac{r^{m+n} \cos{(n-m)\theta}}{m!\, n! \sqrt{\Gamma(m+2)\Gamma(n+2)}} \rho_{n+2,m+2}(x). \tag{36}$$

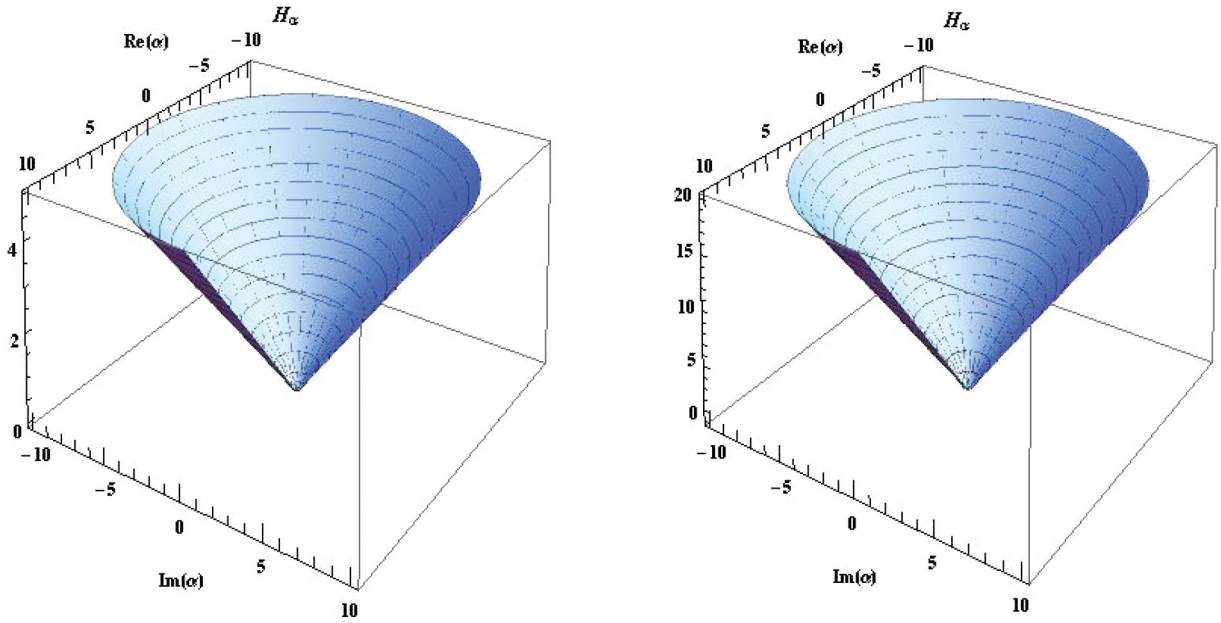

Fig. 8. Mean energy value of eq. (38) for $f(n)=1$, with $k=1$ and the magnetic field intensities $B_0=1/8$ (left) and $B_0=2$ (right).

3.3.3 Discussion

For the graphene coherent states the probability density reaches a maximum which displaces along the x-direction as the parameter $\theta \in [0, \pi/2]$ grows. Also, when $r \to \infty$ we have $\rho(r) \to 0 \; \forall \; \theta$.

The previous behavior can be interpreted as follows. According to the mean values of the position and momentum operators, they can be expressed in terms of the complex eigenvalue α in the way

$$\langle \hat{z} \rangle \sim \mathbf{Re}(\alpha) F_1(|\alpha|), \qquad \langle \hat{p} \rangle \sim \mathbf{Im}(\alpha) F_2(|\alpha|),$$

where $F_{1,2}(|\alpha|)$ are certain functions that depend on the graphene coherent states under study. In particular, when α is real (for $\theta = 0$) we have $\langle \hat{p} \rangle = 0$ which means that, on average, the electron *moves* as many times to the right as to the left, canceling out at the end the positive momentum contributions with the negative ones. Meanwhile, when α is purely imaginary (for $\theta = \pi/2$) we have that $\langle \hat{z} \rangle = 0$. This can be interpreted as if the system would perform symmetric oscillations around the equilibrium position z_0 (or potential center), which is determined by the magnetic field intensity.

On the other hand, when B_0 increases the maximum of the probability density also grows up while their width decreases (due to probability conservation). This means that the electron is to be found in a more bounded region as B_0 grows. An opposite interpretation can be formulated when B_0 decreases.

3.4 Mean energy value

The mean energy value, $\langle \hat{H} \rangle_\alpha$, is another quantity useful to characterize the graphene coherent states.

According to the expansion in eq. (18), where Ψ_n are the eigenfunctions of the Dirac-Weyl Hamiltonian (see eq. (2)), for the graphene coherent states we have that

$$\langle \hat{H} \rangle_\alpha = \sum_{n=0}^{\infty} E_n |a_n|^2 = \hbar v_F \sum_{n=0}^{\infty} \sqrt{n\omega} |a_n|^2. \tag{37}$$

The mean energy value is calculated for each coherent state using this expression, which leads to the following results.

3.4.1 $\langle \hat{H} \rangle_\alpha$ for $f(1) \neq 0$

For the coherent states of eq. (27) we obtain (see fig. 8)

$$\langle \hat{H} \rangle_\alpha = \frac{2\hbar v_F}{2\exp(r^2) - 1} \sum_{n=0}^{\infty} \frac{r^{2n}\sqrt{n\omega}}{\Gamma(n+1)}. \tag{38}$$

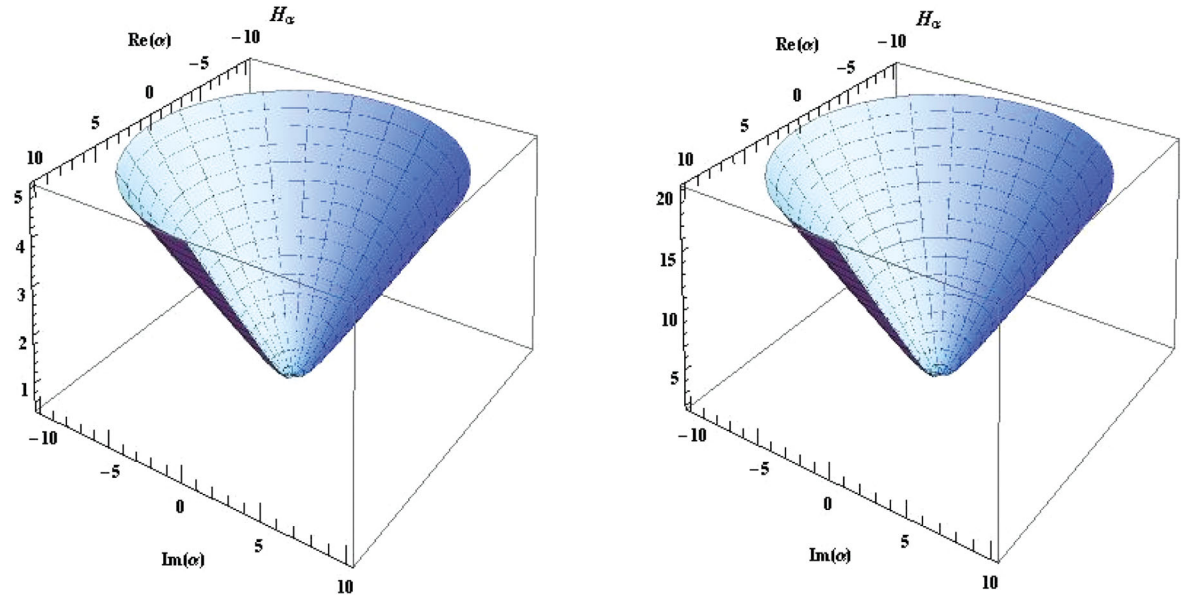

Fig. 9. Mean energy value of eq. (39) for $f(n) = \sqrt{n-1}/\sqrt{n}$, with $k = 1$ and the magnetic field intensities $B_0 = 1/8$ (left) and $B_0 = 2$ (right).

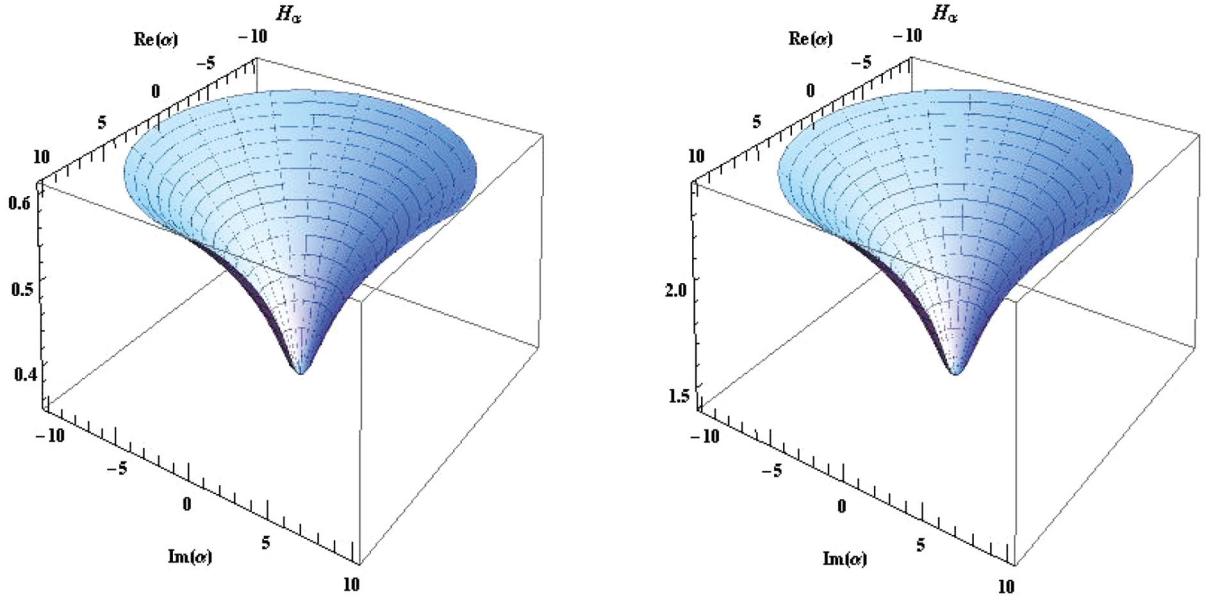

Fig. 10. Mean energy value of eq. (40) for $f(n) = (n-2)\sqrt{n-1}/\sqrt{n}$ with $k = 1$ and the magnetic field intensities $B_0 = 1/8$ (left) and $B_0 = 2$ (right).

3.4.2 $\langle \hat{H} \rangle_\alpha$ for $f(1) = 0$

A. Case with $f(2) \neq 0$.
For the coherent states of eq. (29) we get (see fig. 9)

$$\langle \hat{H} \rangle_\alpha = \hbar v_F \exp(-r^2) \sum_{n=0}^{\infty} \frac{r^{2n}\sqrt{(n+1)\omega}}{\Gamma(n+1)} \,. \tag{39}$$

B. Case with $f(2) = 0$.
Finally, for the coherent states of eq. (31) we arrive at (see fig. 10)

$$\langle \hat{H} \rangle_\alpha = \frac{\hbar v_F}{{}_0F_2(1,2;r^2)} \sum_{n=0}^{\infty} \frac{r^{2n}\sqrt{(n+2)\omega}}{\Gamma[n+2][\Gamma(n+1)]^2} \,. \tag{40}$$

While figs. 8 and 9 have a similar qualitative behavior for $\langle \hat{H} \rangle_\alpha$ as function of α, fig. 10 shows that the mean energy value for the states of eq. (31) grows more slowly than the previous ones. These differences depend once again on the structure of the coherent states taken into account. In addition, according to eq. (37) the mean energy value depends as well on the magnetic field intensity as $\sqrt{B_0}$.

4 Conclusions

Dirac electrons in graphene placed in homogeneous magnetic fields which are orthogonal to the material surface are ideal systems to start implementing the coherent states treatment in solid state physics. In particular, for constant magnetic fields the problem has been addressed for the first time quite recently [27]. In fact, in [27] the same physical configuration of this paper was considered, with the assumption that the magnetic field strenght is strong, in order that the Dirac electron stays always at the $n = 0$ Landau energy level. On the other hand, in this article we are supposing that the magnetic field strenght is not so strong, so that the state of the electron can be a coherent linear combination of all the eigenstates for the Landau energy levels. That is the reason why in this paper we required first to identify the appropriate annihilation and creation operators, in order to build then the coherent states as eigenstates of the former operator. Due to its non-uniqueness, however, it was possible to build different sets of coherent states. Although some of them could look similar to the standard coherent states for the harmonic oscillator, our graphene coherent states in general involve generalized hypergeometric functions. This dependence is more apparent when calculating the Heisenberg uncertainty relation for each set of this paper. This uncertainty achieves a minimum, equal to 1/4, for the coherent states of eq. (27), since the ground state Ψ_0 is involved in this linear combination, while it reaches a maximum for the coherent states of eqs. (29) and (31), depending on the minimum excited state energy involved in the corresponding linear combination (see figs. 2–4).

It is important to remark that, in a sense, the graphene coherent states remind the multiphoton coherent states [36–41], which appear from realizations of the Polynomial Heisenberg Algebras (PHA) for the harmonic oscillator [33–35, 42–44]. In that formalism, the Hilbert space decomposes as a direct sum of m orthogonal subspaces, on each of which it is possible to construct the corresponding coherent states as superpositions of standard coherent states, while in the case of this paper the minimum energy states can be isolated from the remaining Hilbert subspace, depending on the values taken by $f(n)$.

On the other hand, the analysis of the probability density allows to characterize some physical properties of the graphene coherent states. This function indicates that the description for these states remains simple for finite r, whatever the value of the parameter θ is. However, the probability density reaches a maximum whose position along the x-axis actually depends on θ (see figs. 5–7). Meanwhile, the behavior of the mean energy value suggests the possibility of using the graphene coherent states in semi-classical treatments.

Finally, it is important to stress that the non-uniqueness of the annihilation operator leaves open the possibility of exploring more complicated expressions for this operator. As a consequence, plenty of new sets of coherent states can be generated; some of them could be more useful than others for describing interesting physical phenomena in graphene and other carbon allotropes (see, *e.g.*, [45–47]).

This work has been supported in part by the Spanish Junta de Castilla y León and FEDER (Project VA057U16) and MINECO (Project MTM2014-57129-C2-1-P). The authors acknowledge the support of Conacyt. EDB also acknowledges the Conacyt fellowship 290649.

References

1. C. Cohen-Tannoudji, B. Diu, F. Laloë, *Quantum Mechanics*, Vol. **1** (John Wiley & Sons, France, 1977).
2. E. Schrödinger, Naturwissenschaften **14**, 664 (1926).
3. R.J. Glauber, Phys. Rev. **130**, 2529 (1963).
4. R.J. Glauber, Phys. Rev. **131**, 2766 (1963).
5. J.R. Klauder, B.S. Skagerstam, *Coherent States* (World Scientific, Singapore, 1985).
6. A. Perelomov, *Generalized Coherent States and Their Applications* (Springer-Verlag, Berlin, 1986).
7. S.T. Ali, J.P. Antoine, J.P. Gazeau, *Coherent States, Wavelets and Their Generalizations* (Springer-Verlag, New York, 2000).
8. V.V. Dodonov, V.I. Manko (Editors), *Theory of Nonclassical States of Light* (Taylor & Francis, London, 2003).
9. Daniel R. Cooper *et al.*, ISRN Cond. Mat. Phys. **2012**, 501686 (2012).
10. K.S. Novoselov, A.K. Geim, S.V. Morozov, D. Jiang, Y. Zhang, S.V. Dubonos, I.V. Grigorieva, A.A. Firsov, Science **306**, 666 (2004).
11. K.S. Novoselov, A.K. Geim, S.V. Morozov, D. Jiang, M.I. Katsnelson, I.V. Grigorieva, S.V. Dubonos, A.A. Firsov, Nature **438**, 197 (2005).

12. Y.B. Zhang, Y.W. Tan, H.L. Stormer, P. Kim, Nature **438**, 201 (2005).
13. R. Nair, P. Blake, A. Grigorenko, K. Novoselov, T. Booth, T. Stauber, N. Peres, A. Geim, Science **320**, 1308 (2008).
14. T. Enoki, Phys. Scr. T **146**, 014008 (2012).
15. A.H. Castro Neto, F. Guinea, N.M.R. Peres, K.S. Novoselov, A.K. Geim, Rev. Mod. Phys. **81**, 109 (2009).
16. G.W. Semenoff, Phys. Rev. Lett. **53**, 2449 (1984).
17. S. Cahangirov, M. Topsakal, E. Aktrk, H. Şahin, S. Ciraci, Phys. Rev. Lett. **102**, 236804 (2009).
18. A. Fleurence *et al.*, Phys. Rev. Lett. **108**, 245501 (2012).
19. P. Vogt *et al.*, Phys. Rev. Lett. **108**, 155501 (2012).
20. Di Xiao *et al.*, Phys. Rev. Lett. **108**, 196802 (2012).
21. A.F. Andreev, Soviet Physics JETP **19**, 1228 (1964).
22. G.E. Volovik, *Exotic Properties of Superfluid* ^{3}*He* (World Scientific, Singapore, 1992).
23. Y. Hasegawa, R. Konno, H. Nakano, M. Kohmoto, Phys. Rev. B **74**, 033413 (2006).
24. T.O. Wehling, A.M. Black-Schaffer, A.V. Balatsky, Adv. Phys. **63**, 1 (2014).
25. N. Stander, B. Huard, D. Goldhaber-Gordon, Phys. Rev. Lett. **102**, 026807 (2009).
26. E. Diaz-Bautista, D.J. Fernandez C., Eur. Phys. J. Plus **131**, 151 (2016).
27. L.A. Wu, M. Murphy, M. Guidry, Phys. Rev. B **95**, 115117 (2017).
28. S. Kuru, J. Negro, L.M. Nieto, J. Phys.: Condens. Matter **21**, 455305 (2009).
29. B. Midya, D.J. Fernandez, J. Phys. A **47**, 035304 (2014).
30. S.T. Ali, M. Engliš, J.P. Gazeau, J. Phys. A **37**, 6067 (2004).
31. S.T. Ali, F. Bagarello, J. Math. Phys. **49**, 032110 (2008).
32. F. Bagarello, J. Phys. A **42**, 075302 (2009).
33. D.J. Fernandez, V. Hussin, L.M. Nieto, J. Phys. A **27**, 3547 (1994).
34. D.J. Fernandez, L.M. Nieto, O. Rosas-Ortiz, J. Phys. A **28**, 2693 (1995).
35. D.J. Fernandez, V. Hussin, J. Phys. A **32**, 3603 (1999).
36. A.M. Perelomov, Commun. Math. Phys. **26**, 222 (1972).
37. A.O. Barut, L. Giradello, Commun. Math. Phys. **21**, 41 (1971).
38. V. Bužek, I. Jex, T. Quang, J. Mod. Opt. **37**, 159 (1990).
39. V. Bužek, J. Mod. Opt. **37**, 303 (1990).
40. J. Sun, J. Wang, C. Wang, Phys. Rev. A **46**, 1700 (1992).
41. I. Jex, V. Bužek, J. Mod. Opt. **40**, 771 (1993).
42. J.M. Carballo, D.J. Fernandez, J. Negro, L.M. Nieto, J. Phys. A **37**, 10349 (2004).
43. D. Bermudez, D.J. Fernandez, AIP Conf. Proc. **1575**, 50 (2014).
44. M. Castillo-Celeita, D.J. Fernandez, J. Phys: Conf. Ser. **698**, 012007 (2016).
45. V. Jakubsky, S. Kuru, J. Negro, S. Tristao, J. Phys. Condens. Matter **25**, 165301 (2013).
46. V. Jakubsky, S. Kuru, J. Negro, J. Phys. A **47**, 115307 (2014).
47. V. Jakubskym M. Tusek, Ann. Phys. **378**, 171 (2017).